Numerical Evaluation of Porous Structure of Titanium Alloy Fabricated via Selective Laser Melting (SLM) Process

Omar Dhannoon Jumaah[ID], Abdulhaqq A. Hamid*[ID], A. D. Younis[ID]

Department of Mechanical Engineering, University of Mosul, Mosul 41002, Iraq

Corresponding Author Email: abdulhaqqhamid@uomosul.edu.iq

ABSTRACT

Selective laser melting (SLM) has attracted more attention as a promising additive manufacturing technique to manufacture porous structures. The porous structure of Ti6Al4V alloy manufactured by the SLM process has been attracted more attention due to its excellent characteristics in biomedical applications. However, the presence of pores within the porous structure can critically impact the performance and mechanical properties of the final structure. The numerical simulation is conducted to examine the influence of pores on the mechanical behavior of Ti-alloy porous structures. The effect of volume-based porosity in the range of (63.8-76.6 vol.%) on porous structure is investigated using a 3D finite element model created by ANSYS software. The uniaxial compression testing is done to determine the effectiveness of mechanical properties for several porous samples, showing an exponential decreasing trend with increasing porosity content. The finite element analysis shows good agreement with experimentally obtained results. It also helps in determining mechanical properties limits of porous structure to be compatible with the human bone. Finally, the results obtained from this numerical study allow for clear insights into both the design and optimization of porous structures fabricated via the SLM process, contributing to the advancement of additive manufacturing for Ti-alloys in many engineering applications.

1. INTRODUCTION

Porous materials have been attracted more attention due to their excellent characteristics in biomedical applications, such as repairing and replacing damaged bones and scaffolds. Porous structure implants can establish good fixation with surrounding tissue that grows into and through a porous matrix. Metal additive manufacturing (AM) techniques provide a dramatic solution to generate complex porous structure implants. One of the essential methods of (AM) is to perform a selective process based on laser melting, which has the benefit of designing and manufacturing three-dimensional porous implants to mimic bone characteristics [1].

SLM technology fuses sequential layers upon layers of metal powder to fabricate implant geometry by using a high-energy laser. The laser beam tracks precisely a sliced CAD data to fuse metal powder layers for forming the final part [2]. 3D solid functional parts are widely generated by the SLM technique [3]. The presence porous structure in implants enhances the bone ingrowth and the fixation of implant with the host bones. The regeneration of bone tissue can create a mechanical interconnect between the bone and the fabricated implant. Tiny pores can hinder the bone ingrowth due to pore blockage, whereas big pores may reduce the cell adhesion surface area and weight-bearing capacity [4]. Thus, adjusting the pore size and porosity percentage is efficient for bone

ingrowth. Customizing the porous structure of the biomaterial can provide proper mechanical properties to withstand physiological loads [5]. Integrating a porous implant into the femoral stem assists in reducing the stiffness and mitigates the stress-shielding effect [6]. The matching of porous structures biomedical and mechanical properties with natural bones properties is a significant challenge in orthopedic implants [7]. Bones typically exhibit anisotropy, meaning they have varying stiffness and strength depending on the direction. As a result, porous metals that mimic the stiffness of adjacent bones can effectively transfer loads and reduce the stress shielding phenomenon [8].

For comparison, natural bone has Young's modulus (10-30 GPa) while bulk Titanium alloys have nearly (110 GPa); bone is insufficiently loaded leads to a stress shielding effect which is causing bone resorption over time and implant failure [9]. The tendency of elastic modulus for the porous Ni-Ti implant with embrace bone can be minimized. A porous Ni-Ti sample with 35.5% porosity shows an elastic modulus of 28 GPa nearly equals the elastic modulus of natural bones. Consequently, a porous Ni-Ti implant can be matched well with surrounding bone and avoid stress-shielding that causes the implant to fail.

SLM process adjusts the porosity or relative density of biomaterials to overcome Young's moduli mismatch with the surrounding bone. Porous Ti6Al4V implants manufactured by

SLM are biocompatible and they recommended for in vitro cell proliferation [10]. High biocompatibility, mechanical properties, and corrosion resistance of Ti6Al4V alloys are required in many biomedical applications to perform for replacing damage of bone tissue [11]. By adjusting the porosity content, pore size, shape, and distribution, the mechanical properties and characteristics of porous implants can be fine-tuned and enhanced [12].

A previous study [5] analyzed the influence of shape, pore size, and permeability on bone scaffolds made of Ti6Al4V alloys. For this purpose, six different structures were fabricated by SLM, which included pore shapes (triangular, rectangular, and hexagonal) and pore sizes (500 μm and 1000 μm). A qualitative examination of the Ti6Al4V structure using SEM showed that a structure with 500 μm pore size had higher cell growth on the edges. The pore shape leads to distribute cells with high density in the corners.
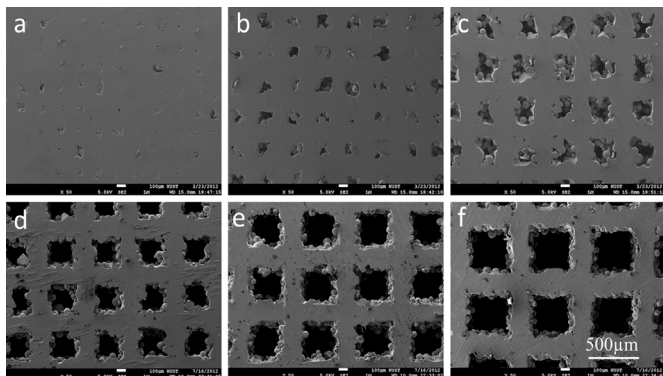

Figure 1. SEM images of porous Ti6Al4V implants created by SLM with different scan line spacing: (a) 200 μm; (b) 300 μm; (c) 400 μm; (d) 500 μm; (e) 600 μm and (f) 700 μm [2]

The impact of pore size on bone ingrowth is still a debated topic in the scientific literature [13]. Therefore, the pore size should not exceed 500 μm to meet the pore size requirements for human bone [14]. In contrast, the scan line spacing affects the pore properties and mechanical properties of porous structures. Thus, it should be larger than 500 μm to obtain implants with interconnected pores, as shown in Figure 1. Also, the bulk powder must be able to flow through the passage structure to achieve a porous structure [2]. As a result,

adjusting the distance between scan lines prevents overlapping between individual lines and ensures that the pore size is large enough. Tiny pore size may inhibit powder particles from passing through the pores and produce disconnected zones.

Setting SLM process parameters has a crucial role in the successful construction of porous implant structures, including their microstructure, mechanical properties, and biological performance. These parameters can be related to laser, scan, powder, and temperature. By carefully adjusting and optimizing these parameters, the desired characteristics of porous implants can be achieved.

Porous metals that are suitable will have a similar stiffness to the surrounding bones, which makes them useful for transferring loads and reducing the stress-shielding effect [9]. Though increased porosity may lead to enhancement of the biological processes, it can have a negative impact on the stiffness and strength. The structure of the implants is greatly influenced by the distribution of stress and the effective stiffness. Thus, finite element model is used to investigate the mechanical properties limits of porous implants that are compatible with human bones. The current study evaluates the porosity content effects on mechanical properties of Ti6Al4V porous structure by using a 3D finite element model.

2. MATERIALS AND METHODS

SLM technology involves using a high-intensity laser to fuse metal powders layers, as shown in Figure 2. SLM fabricates very complex implants with the possibility of precisely adjusting surface roughness and porosity. The thickness of the layer, which is cut into a specific horizontal film, is controlled by a CAD model. The average layer thickness ranges between 30 μm and 150 μm, depending on the particles of the material. Each layer is supplied in a powder state and then melted by a laser that is guided using a scanner to the specified coordinates of the part geometry. The process is repeated by adding successive layers of material until the desired implant is manufactured [15]. The SLM technology allows the powder material to be completely melted, producing completely dense mesh-like components without additional post-processing. This process is performed in a container full with an inert gas such as nitrogen (N_2) or argon (Ar) to protect hot metal parts from oxidation [16].
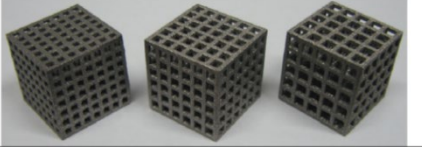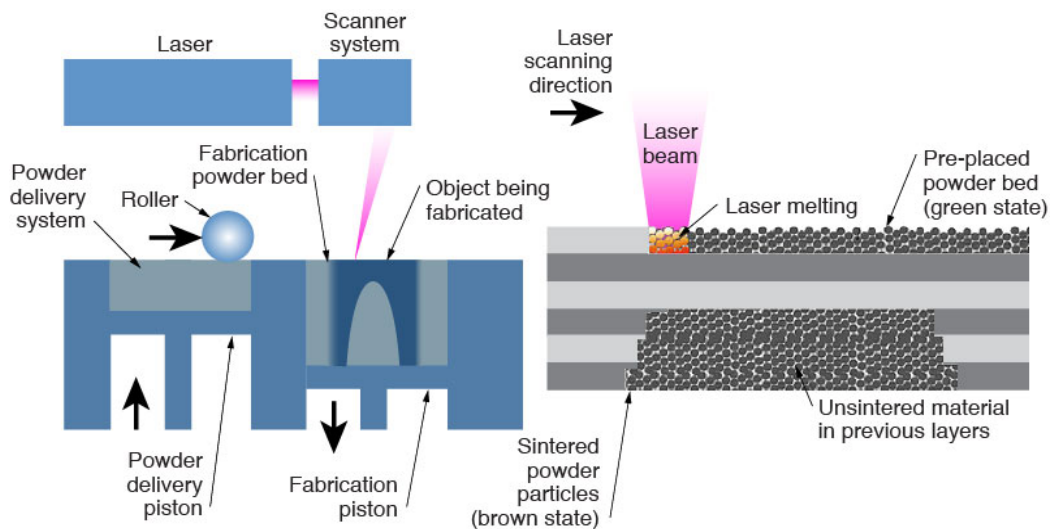

Figure 2. Schematic of the SLM process [15]

3. MATERIAL PROPERTIES

Titanium alloy (Ti6Al4V) is commonly used in biomedical applications. Table 1 provides a detailed overview of the mechanical and physical properties of the (Ti6Al4V) alloy [17]. In order to make an accurate comparison with the numerical model, the geometry of previously manufactured porous parts (as shown in Figure 3) was reproduced by the SLM technique as reported in a study [18]. EOSINT M 270 rapid manufacturing system (EOS, Germany) was used to fabricate porous parts. Zwick Roell 1474 testing machine has a load capacity of 100 kN was used to determine the compressive loads of the porous Ti6Al4V structure.

Table 1. Mechanical and physical properties of Ti6Al4V alloy used for the numerical model [17]

Density (kg/m³)	4429	Elastic Modulus (GPa)	110
Yield strength (MPa)	945.7	Poisson's ratio	0.33
Ultimate strength (MPa)	980	Melting point (°C)	1655

Sets of porous structure parts			
Pore size (μm)	1428±42	1741±38	2209±45
Strut (μm)	611±23	617±22	641±31
Pore number	7x7	6x6	5x5
Porosity %	63.8	70.7	76.6
Stiffness (GPa)	8.73±0.07	7.72±0.04	5.5±0.3
Yield (MPa)	170±5	129±4	93±3
Strength (MPa)	219±5	163±2	108±3

Figure 3. Experimental data of porous parts fabricated by a low energy input SLM process [18]

The structure's porosity was defined using the bulk density equation Eq. (1) based on mean dimensional measurements, as well as measuring the mass of the sample using a digital scale.

$$\emptyset = 1 - \frac{M/V_b}{\rho} \tag{1}$$

where, $\emptyset$ is the structure's porosity, M is the mass (g), V_b is the volume (mm³), and ρ is the density (g/mm³).

4. COMPONENT DESIGN

Three-dimensional cubic models (15 mm, V_b=3375 mm³) of porous, cellular structures with porosity (63.8-76.6%) were adapted from the study by Sallica-Leva et al. [18]. The CAD models were reproduced for numerical analysis to accurately compare the porous fractions obtained by SLM and FEM models. The finite element modeling software ANSYS was used to predict the mechanical properties of individual porous structures. The porous parts were modeled using solid tetrahedron elements with a mesh size of 0.2 mm to capture the solution accurately. Since the FE model of porous structure is mainly dependent on the material model. Thus, the bilinear isotropic hardening model was used to describe the material behavior of Ti6Al4V porous structures under compressive loads. The bottom surface of the model was fixed, and the downward force was applied to the top surface. With each load cycle, the applied force was progressively increased until the

total deformation reached 0.6 mm. It is assumed that the model is homogeneous and possesses identical strut sizes, as depicted in Figure 4. Eq. (2) shows the calculation for the porosity of the selected cellular structure.

$$\emptyset = \frac{V_p}{V_b} \tag{2}$$

where, V_p is the volume of pores and V_b is the volume of bulk structure. The porosity was varied by increasing the pore size. Increasing the porosity leads to fewer pores on the sample's face as given in Table 2.

Table 2. CAD models characterization and dimensions

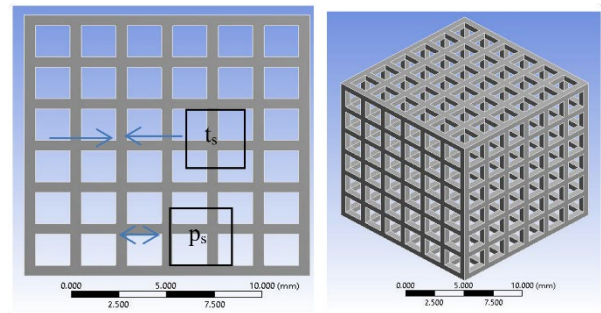| Sample	Ø %	p_s (mm)	t_s (mm)	Vp (mm³)
Set 1	63.8	1.445	0.611	2153
Set 2	70.7	1.57	0.617	2386
Set 3	76.6	2.04	0.641	2585

Figure 4. Three-dimensional cubic samples with porosity content of 70.7%, strut size t_s of 0.611 mm, and pore size p_s of 1.445 mm

A comparative study with experimental work was conducted to determine the accuracy of the numerical model. The obtained numerical results were compared with both experimental results published in a study [18] and the theoretical model of Gibson and Ashby [19]. The mechanical properties of porous structures were calculated based on relative densities by applying theoretical model formulas:

$$\sigma_y = \sigma_{y0} \times [1 - \emptyset]^{1.5} \tag{3}$$

$$\sigma_{max} = \sigma_{max0} \times [1 - \emptyset]^{1.5} \tag{4}$$

$$E_{eff} = E_0 \times [1 - \emptyset]^2 \tag{5}$$

where, σ_y is yield strength, σ_{max} is the ultimate strength and E_{eff} is an effective modulus of the porous material. Also, σ_{y0} is bulk material's yield strength, σ_{max0} is ultimate and E_0 is elastic modulus.

5. RESULTS AND DISCUSSION

The numerical model was used successfully to explore the porosity content impact on the mechanical properties of Ti6Al4V porous structure that is fabricated by the SLM process. Thus, the equivalent stress-strain curves for Ti6Al4V porous structures with porosity content (63.8-76.6%) were plotted, as shown in Figure 5. When the solution is converged, effective stress (E_{eff}), yield strength (σ_y), and ultimate

compressive strength were determined using FEA simulation of all samples with various porosity contents.
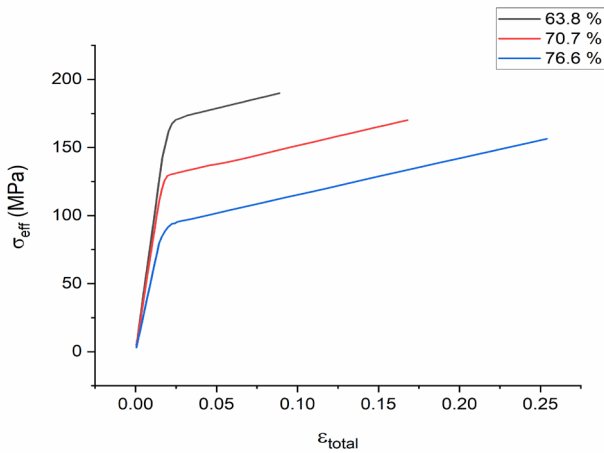

Figure 5. The effective stress-strain curve of different porosity contents

The numerical results showed a good match with the experimental results conducted by a study [18] for the effective stress and yield strength, respectively. However, the experimental values of ultimate compressive strength (219 MPa-108 MPa) were higher than the values simulated by the FE model. It was noted that the numerical values of ultimate compressive strength of all specimens were in the range (192 MPa-116 MPa) at 10% equivalent total strain. This difference could be due to cell surface curvatures and waviness resulting from subsequent solidification due to cooling of the titanium alloy powder from fusion at elevated temperatures. These deformations in the entire sample may lead to local heterogeneities and stress concentrations that significantly affect the hardness and strength of the porous structures [20]. In addition, research indicates that precise physical behavior and actual boundary conditions play a critical role in achieving matching results.

The theoretical results obtained through the Gibson and Ashby model [19] showed higher values than the experimental measurements of the porous structure as shown in Figure 6. This discrepancy between theoretical and practical values could be due to the surface undulations on the solid Ti6Al4V structure, according to the observations in the study [9]. The decrease in effective hardness and compressive strength produced by the part is consistent with expectations for cellular solids with increased porosity. However, a significant decrease in the compressive strength of the porous structure was observed when its porosity reached (76.6%) compared to its porosity (63.6%).

Under compressive loading, the von Misses stress distribution in porous structure is shown in Figure 7. The maximum stress value is in the range of (189-165 MPa) for all samples. It is observed that the stress concentration increased with increasing the porosity contents. It is indicated that porous structures with porosity (Φ=63.6%) exhibited maximum von Mises stress (189 MPa) compared with other structures. The compressive ultimate strength decreased significantly with increasing porosity content. Figure 8 shows the values of the stress concentration and safety factors related to the porosity content. Interestingly, the stress was primarily located vertically at the center of the struts, which indicates that a low safety factor value occurs at the vertical strut for all

samples. Thus, the probability of the strut failure at the middle point was maximum because the vertical struts were the least supported. This is mainly due to the differences in the truss design of the porous structure samples. Figures 8(a)-(c) show the safety factor values for the internal joint of the unit cell in the porous structures. This confirms that the ultimate strength of porous structure depends on the strut size located far from the porosity.
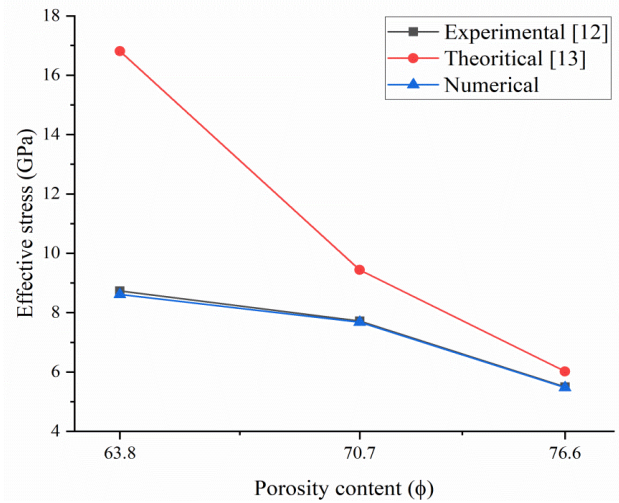
(a)
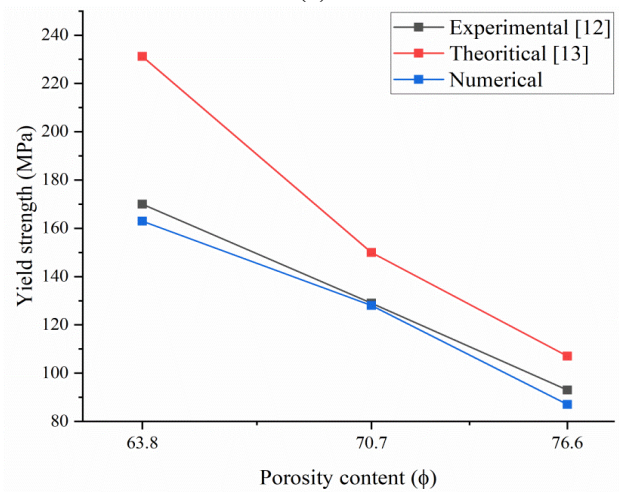
(b)
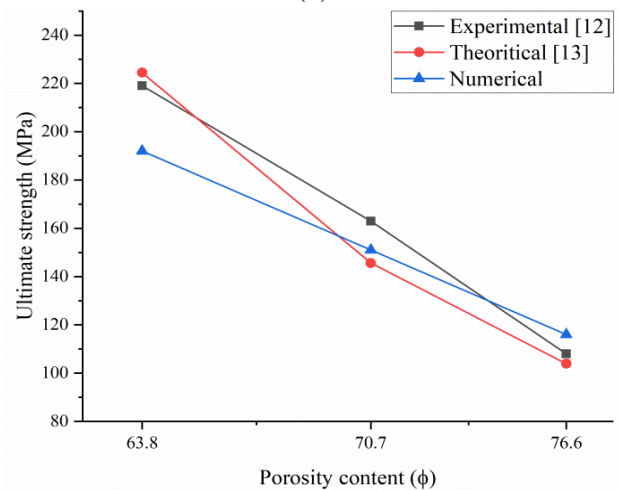
(c)

Figure 6. Mechanical properties of the porous parts obtained experimentally [18] and theoretical and numerical models
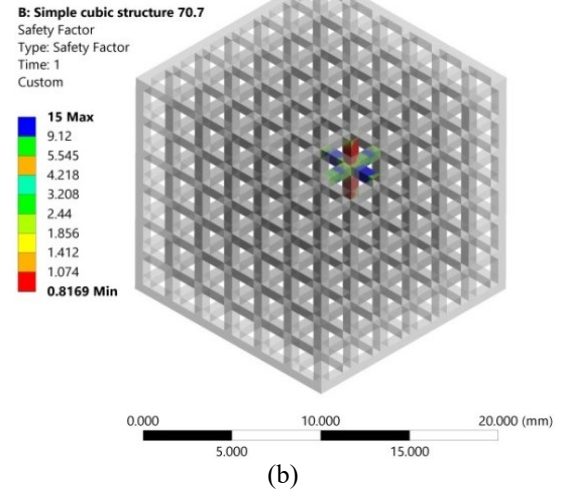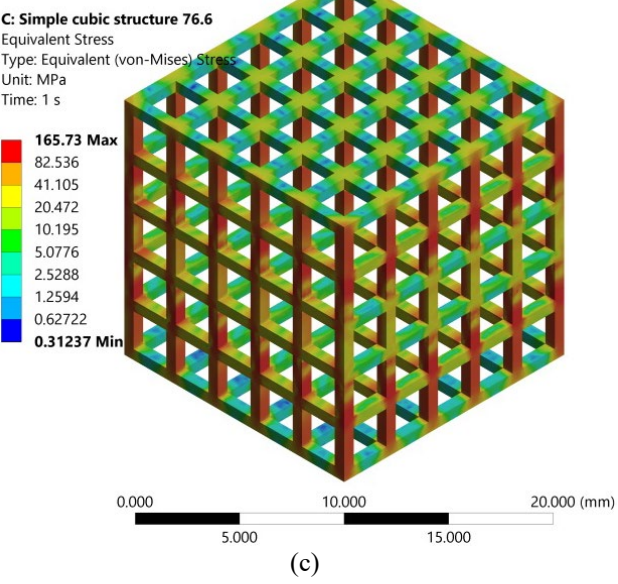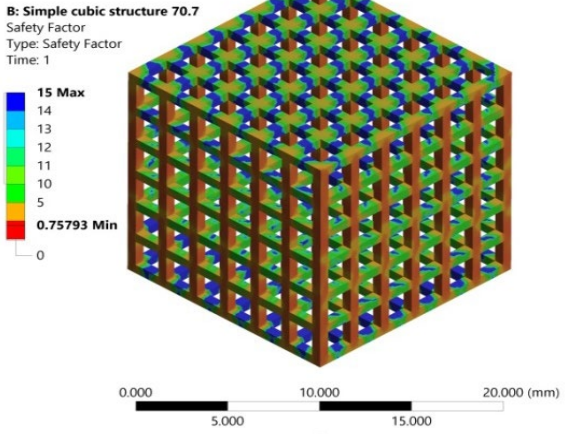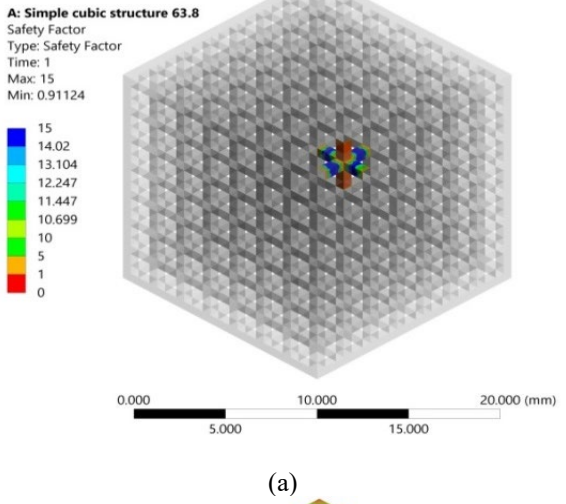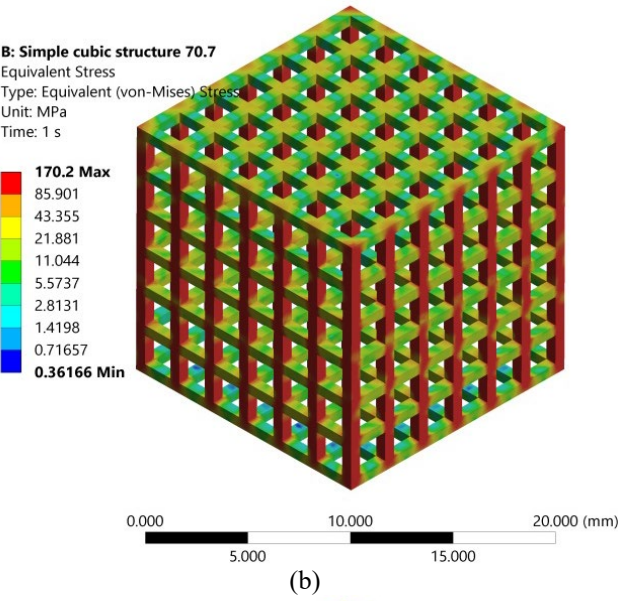
(a)

(b)

(c)

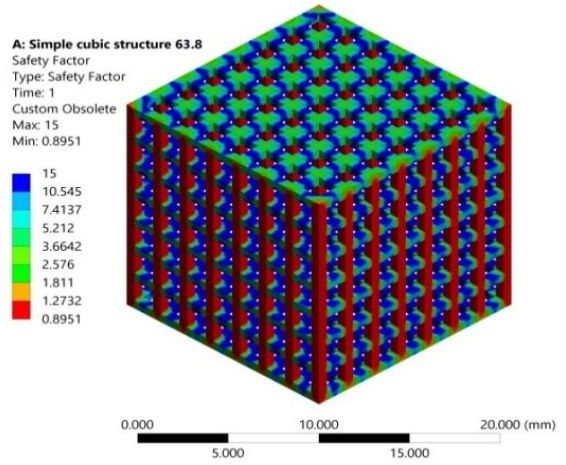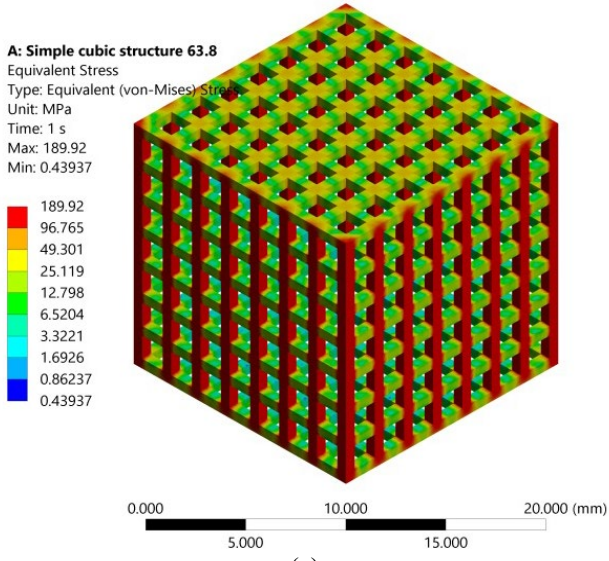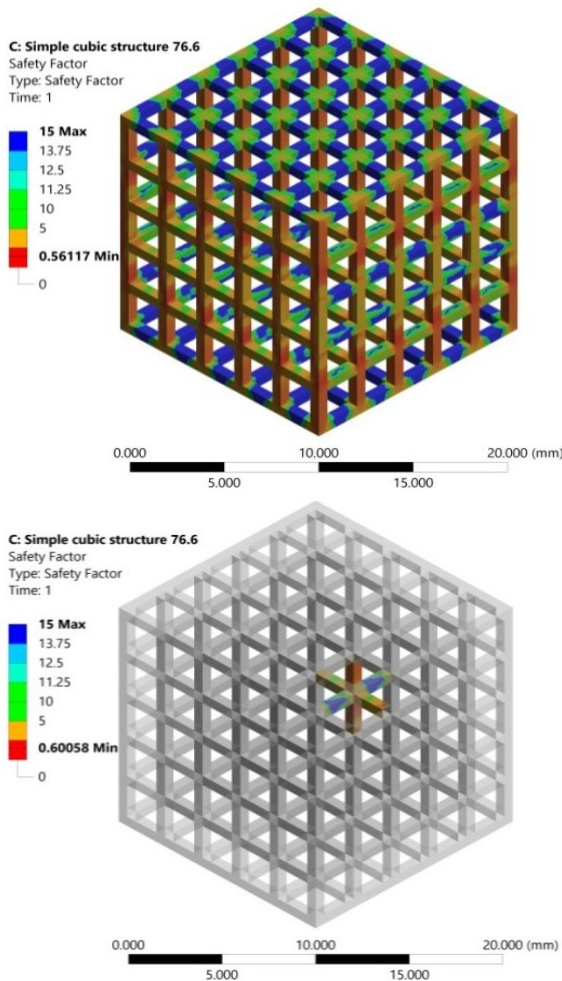**Figure 7.** FEA contour plot for the distribution of equivalent Von Mises stress with various porosity content (a-Φ=63.8%, b-Φ=70.7%, and c-Φ=76.6%)

(a)

(b)

(c)

Figure 8. FEA contour plot for the stress concentration and safety factor for porosity contents (a-Φ=63.8%, b-Φ=70.7%, and c-Φ=76.6%)

6. CONCLUSIONS

This current study created a validated FE model to evaluate the mechanical properties of Ti6Al4V porous structures manufactured using the SLM process. The 3D numerical model is successfully used to simulate equivalent stress, yield stress, and ultimate strength of samples containing different porosities (63.8, 70.7, and 76.6%) under compressive loading. The numerical results of elastic modulus and yield strength showed good agreement with the experimental values. Interestingly, the vertical strut for all samples shows maximum stress concentration in the middle, which increases the probability of failure at these points. It has been observed that both the overall porosity and the dimensions of the struts consistently affected the mechanical properties of porous structures. These observations highlight the importance of considering the porosity and strut dimension when analyzing and predicting the mechanical behavior of such structures.

REFERENCES

[1] Yap, C.Y., Chua, C.K., Dong, Z.L., Liu, Z.H., Zhang, D.Q., Loh, L.E., Sing, S.L. (2015). Review of selective laser melting: Materials and applications. Applied Physics Reviews, 2(4): 041101, https://doi.org/10.1063/1.4935926

[2] Zhang, S., Wei, Q., Cheng, L., Li, S., Shi, Y. (2014). Effects of scan line spacing on pore characteristics and mechanical properties of porous Ti6Al4V implants fabricated by selective laser melting. Materials & Design, 63: 185-193. https://doi.org/10.1016/j.matdes.2014.05.021

[3] Fu, C.H., Guo, Y.B. (2014). Three-dimensional temperature gradient mechanism in selective laser melting of Ti-6Al-4V. Journal of Manufacturing Science and Engineering, 136(6): 061004. https://doi.org/10.1115/1.4028539

[4] Zaharin, H.A., Abdul Rani, A.M., Azam, F.I., Ginta, T.L., Sallih, N., Ahmad, A., Yunus, N.A., Zulkifli, T.Z.A. (2018). Effect of unit cell type and pore size on porosity and mechanical behavior of additively manufactured Ti6Al4V scaffolds. Materials, 11(12): 2402. https://doi.org/10.3390/ma11122402

[5] Van Bael, S., Chai, Y.C., Truscello, S., Moesen, M., Kerckhofs, G., Van Oosterwyck, H., Kruth, J.P., Schrooten, J.J.A.B. (2012). The effect of pore geometry on the in vitro biological behavior of human periosteum-derived cells seeded on selective laser-melted Ti6Al4V bone scaffolds. Acta Biomaterialia, 8(7): 2824-2834. https://doi.org/10.1016/j.actbio.2012.04.001

[6] Liu, B., Wang, H., Zhang, N., Zhang, M., Cheng, C.K. (2021). Femoral stems with porous lattice structures: A review. Frontiers in Bioengineering and Biotechnology, 9: 772539. https://doi.org/10.3389/fbioe.2021.772539

[7] Ryan, G., Pandit, A., Apatsidis, D.P. (2006). Fabrication methods of porous metals for use in orthopaedic applications. Biomaterials, 27(13): 2651-2670. https://doi.org/10.1016/j.biomaterials.2005.12.002

[8] Wang, X., Xu, S., Zhou, S., Xu, W., Leary, M., Choong, P., Qian, M., Brandt, M., Xie, Y.M. (2016). Topological design and additive manufacturing of porous metals for bone scaffolds and orthopaedic implants: A review. Biomaterials, 83: 127-141. https://doi.org/10.1016/j.biomaterials.2016.01.012

[9] Parthasarathy, J., Starly, B., Raman, S., Christensen, A. (2010). Mechanical evaluation of porous titanium (Ti6Al4V) structures with electron beam melting (EBM). Journal of the Mechanical Behavior of Biomedical Materials, 3(3): 249-259. https://doi.org/10.1016/j.jmbbm.2009.10.006

[10] Hollander, D.A., Von Walter, M., Wirtz, T., Sellei, R., Schmidt-Rohlfing, B., Paar, O., Erli, H.J. (2006). Structural, mechanical and in vitro characterization of individually structured Ti-6Al-4V produced by direct laser forming. Biomaterials, 27(7): 955-963. https://doi.org/10.1016/j.biomaterials.2005.07.041

[11] Arefin, A.M., Lahowetz, M., Egan, P.F. (2021). Simulated tissue growth in tetragonal lattices with mechanical stiffness tuned for bone tissue engineering. Computers in Biology and Medicine, 138: 104913. https://doi.org/10.1016/j.compbiomed.2021.104913

[12] Che Ghani, S.A., Harun, W.S.W., Mat Taib, Z.A., Ab Rashid, F.F., Hazlen, R.M., Omar, M.A. (2016). Finite element analysis of porous medical grade cobalt chromium alloy structures produced by selective laser melting. Advanced Materials Research, 1133: 113-118. https://doi.org/10.4028/www.scientific.net/AMR.1133.1

13

[13] Torres-Sanchez, C., Al Mushref, F.R.A., Norrito, M., Yendall, K., Liu, Y., Conway, P.P. (2017). The effect of pore size and porosity on mechanical properties and biological response of porous titanium scaffolds. Materials Science and Engineering: C, 77: 219-228. https://doi.org/10.1016/j.msec.2017.03.249

[14] Taniguchi, N., Fujibayashi, S., Takemoto, M., Sasaki, K., Otsuki, B., Nakamura, T., Matsushita, T., Kokubo T., Matsuda, S. (2016). Effect of pore size on bone ingrowth into porous titanium implants fabricated by additive manufacturing: An in vivo experiment. Materials Science and Engineering: C, 59: 690-701. https://doi.org/10.1016/j.msec.2015.10.069

[15] King, W.E., Anderson, A.T., Ferencz, R.M., Hodge, N.E., Kamath, C., Khairallah, S.A., Rubenchik, A.M. (2015). Laser powder bed fusion additive manufacturing of metals; physics, computational, and materials challenges. Applied Physics Reviews, 2(4): 041304, https://doi.org/10.1063/1.4937809

[16] Li, R., Liu, J., Shi, Y., Wang, L., Jiang, W. (2012). Balling behavior of stainless steel and nickel powder during selective laser melting process. The International Journal of Advanced Manufacturing Technology, 59: 1025-1035. https://doi.org/10.1007/s00170-011-3566-1

[17] Hammer, J.T. (2012). Plastic deformation and ductile fracture of Ti-6Al-4V under various loading conditions. Master's Thesis, The Ohio State University. http://rave.ohiolink.edu/etdc/view?acc_num=osu1354700435.

[18] Sallica-Leva, E., Jardini, A.L., Fogagnolo, J.B. (2013). Microstructure and mechanical behavior of porous Ti-6Al-4V parts obtained by selective laser melting. Journal of the Mechanical Behavior of Biomedical Materials, 26: 98-108. https://doi.org/10.1016/j.jmbbm.2013.05.011

[19] Gibson, L.J., Ashby, M.F. (1997). Cellular solids: Structure and properties. Cambridge University Press. https://doi.org/10.1017/CBO9781139878326

[20] Simone, A.E., Gibson, L.J. (1998). The effects of cell face curvature and corrugations on the stiffness and strength of metallic foams. Acta Materialia, 46(11): 3929-3935. https://doi.org/10.1016/S1359-6454(98)00072-X

NOMENCLATURE

SLM	Selective Laser Melting
M	the mass, g
V_p	the volume of pores, mm^3
V_b	the volume of bulk structure, mm^3
t_s	strut size, mm
p_s	pore size, mm
N_2	the nitrogen gas
Ar	the argon gas

Greek symbols

$\emptyset$	the porosity of the sample
P	the density, g.mm^{-3}
σ_y	the yield strength, MPa
σ_{y0}	the bulk material's yield strength, MPa
σ_{max}	the ultimate strength, MPa
σ_{max0}	the bulk material's ultimate strength, MPa
E_{eff}	the porous material's effective modulus, GPa
E_0	the elastic modulus, GPa

Subscripts

P	pores
B	bulk
S	strut
Y	yield
Max	maximum
Eff	effective